Ab-initio investigation on the electronic and thermoelectric properties of new half-Heusler compounds KBiX (X = Ba and Sr)

Z Meghoufel, F Cherifi, A Boukra, F Terki

Ab-initio investigation on the electronic and thermoelectric properties of new half-Heusler compounds KBi*X* (*X* = Ba and Sr)

Z F Meghoufel[1] F Cherifi[1], A Boukra[1] and F Terki[2,*]

[1] Laboratoire de Structure, Elaboration et Application des Matériaux Moléculaires, SEA2M, Université Abdelhamid Ibn Badis, Mostaganem, Algeria
[2] Physiologie et Médecine Expérimentale du Cœur et des Muscles PhyMedExp, Université de Montpellier, INSERM U1046, CNRS UMR 9214, CHU Arnaud de Villeneuve 371 avenue du Doyen Gaston Giraud, 34295 Montpellier, Cedex 5, France

E-mail: ferial.terki@umontpellier.fr

Abstract

Electronic structures and thermoelectric (TE) properties of KBiBa and KBiSr half-Heusler compounds are investigated by using the combined framework of first-principles and semi-classical Boltzmann transport theory. Elastic and phonon properties calculations reveal that these compounds are mechanically and dynamically stable. Band structures calculations, using the Tran and Blaha modified Becke–Johnson potential including spin–orbit coupling, show that KBiBa and KBiSr compounds are semiconductors with an indirect bandgap of 0.88 and 0.95 eV respectively. Performing calculations on lattice thermal conductivity, deformation potential, effective mass of charge carriers and their relaxation times allow us to deduce the dependence of the figure of merit ZT on doping concentration and temperature. At 1200 K, KBiBa and KBiSr compounds exhibit a ZT peak value of 2.68 and 1.56 at optimized *n*-doping values of 2.2×10^{19} and 1.7×10^{19} cm^{-3}, respectively. Considering high ZT values, KBiBa and KBiSr are considered to be ideal TE candidates at high temperature.

Keywords: half-Heusler, thermoelectric properties, first-principles, spin-orbit coupling, figure of merit

(Some figures may appear in colour only in the online journal)

1. Introduction

Thermoelectric (TE) materials have attracted much attention during the last decade thanks to their ability to transform heat to electrical energy [1]. The efficiency of TE conversion lies in the dimensionless figure of merit ZT given by $\mathrm{ZT} = \frac{S^2\sigma}{\kappa}T$, where S is the Seebeck coefficient depending on the effective mass of charge carriers, as well as on their concentrations. σ is the electrical conductivity, T the absolute temperature and κ the total thermal conductivity, which is the sum of the electronic and the lattice contribution parts ($\kappa_e + \kappa_L$). Good TE performances can be obtained by increasing electrical properties such as electrical conductivity and Seebeck coefficient to enhance the power factor ($S^2\sigma$), and at the same time reducing the thermal conductivity, which is an important feature describing thermal losses by electrons and phonons diffusion. The above mentioned parameters are interdependent, implying difficulties to enhance ZT. Thus, the main challenge lies in the manner to improve one of them without affecting the others.

Both 18 and 8 valence electrons half-Heusler materials have been investigated and developed for various TE applications.

* Author to whom any correspondence should be addressed.

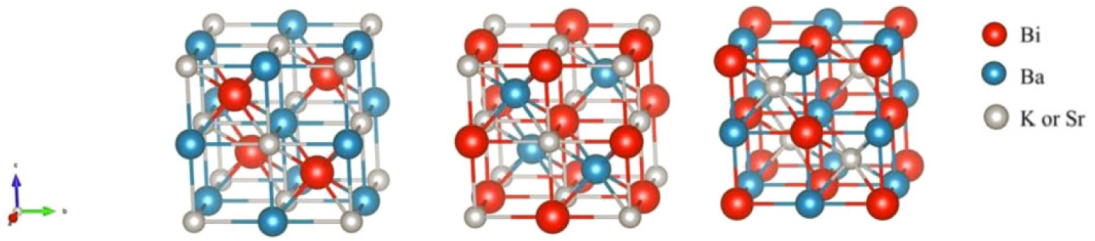

Figure 1. Three phases of the half-Heusler alloys KBiX, α phase (left), β phase (middle) and γ phase (right).

Most of them are expected to operate efficiently at high temperature range (beyond 900 K). Recently, Guo *et al* [2] selected among a set of 95 starting compounds nine p-type and six n-type half-Heusler compounds with high power factors. They found high ZT values of 2.46 and 2.11 for p-type VCoGe and NbCoSi, respectively, at 900 K. The half-Heusler NbFeSb compound has been studied with and without doping [3]. The figure of merit of undoped NbFeSb exceeds 1, whereas a p-doped NbFeSb reaches a ZT of 1.5 at 1200 K. This result was explained by the fact that doping sites enhance point-defect and electron–phonon scattering, reducing the thermal lattice conductivity. Fang *et al* [4] predicted, theoretically, a ZT of 1.5 at 1200 K for p-type RuTaSb half-Heusler, resulting from low effective mass and high band degeneracy. TE properties of I–II–V half-Heusler compounds XMgN (X = Li, Na, K) were studied theoretically by Rashid Ahmed *et al* [5]. ZT was approximately found equal to 1 for all n-doped compounds. However, only electronic thermal conductivity to relaxation time ratio was taken into account, omitting the phonons interactions and diffusion phenomena that can occur. This can induce large discrepancies with the real value of the figure of merit. Sun *et al* [6] studied TE properties of II–III–III half-Heusler compounds BXGa (X = Be, Mg, and Ca). A remarkable high ZT value of 7.38 was predicted for the n-type BCaGa at 700 K. Zhang *et al* calculated TE performance of two semiconductors BaBiNa and SrBiNa, combining the first-principle DFT with the semi-classical Boltzmann transport theory [7]. Maximum ZTs of 1.14 and 1.16 were reached for n-type BaBiNa and SrBiNa at carrier concentrations of 5.62×10^{18} and 3.60×10^{18} cm^{-3} at 800 K, respectively.

Relaxation time and lattice thermal conductivity are crucial parameters to accurately assess the figure of merit. Yang *et al* [8] used the constant relaxation time approximation (CRTA) to predict TE properties of 36 p- and n-type half-Heusler compounds. Guo *et al* [2] used both the CRTA and the deformation potential (DP) approximations to examine electrical conductivities of nine p-type and seven n-type half-Heusler compounds. They conclude that the CRTA method underestimates considerably the electrical conductivity value. Carrete *et al* [9] investigated approximately 79 000 half-Heusler compounds using a combination of machine learning techniques and *ab initio* calculations. They selected 75 thermodynamically stable compounds and found among them only three semiconductors having thermal conductivities lower than 5 W m^{-1} K^{-1}. Thereafter, Toher *et al* [10] used the automatic

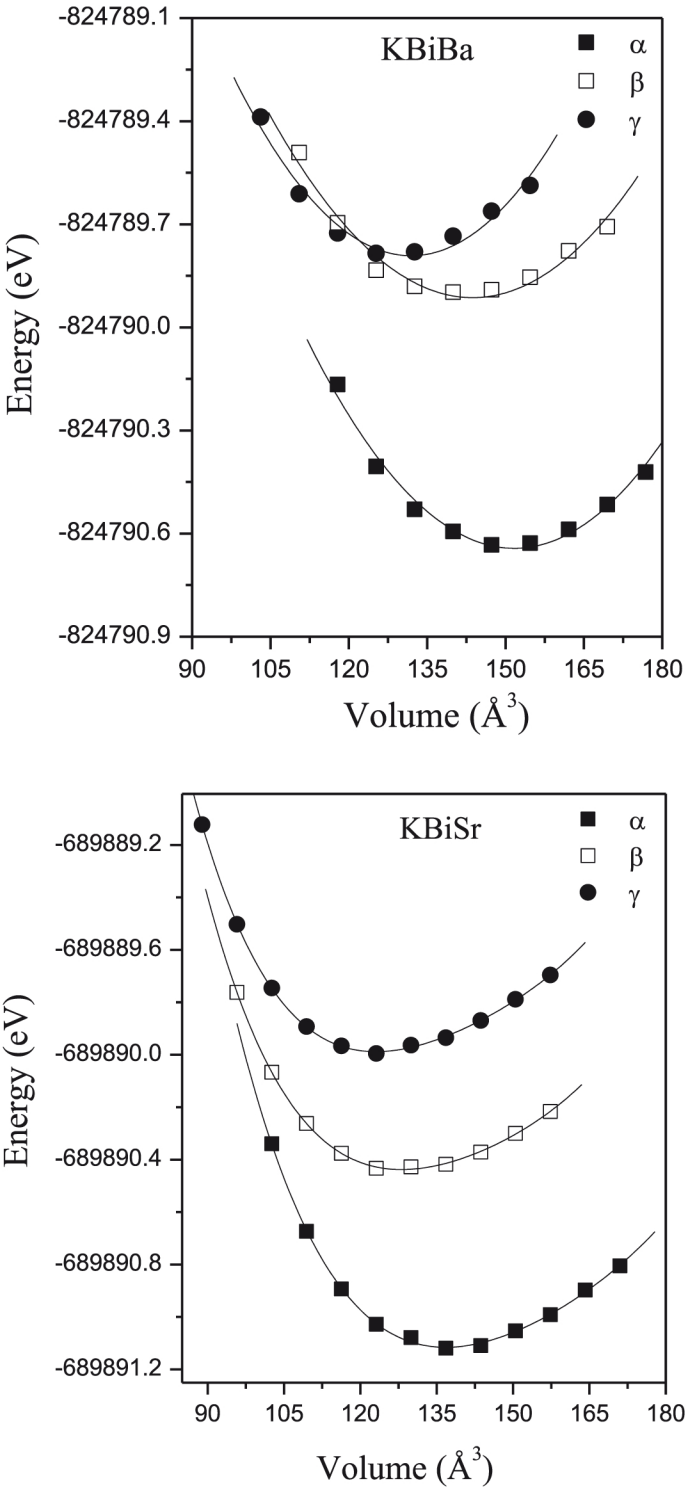

Figure 2. Calculated total energy versus volume for α, β, and γ phases of KBiBa and KBiSr.

Table 1. Calculated equilibrium lattice parameter, bulk modulus, its pressure derivative and bandgap energy of KBiBa and KBiSr compounds using SOC and SOC + mBJ.

Compound		a_0 (Å)	B_0 (GPa)	B_0'	Gap (eV)
KBiBa	SOC	8.40	16.69	3.83	0.30
	SOC + mBJ				0.88
					0.75[a]
	Other calc.	8.45[a]			0.70[b]
KBiSr	SOC	8.18	17.18	4.03	0.42
	SOC + mBJ				0.95
	Other calc.				0.49[b]

[a][19].
[b][2].

Gibbs library (AGL) in order to estimate thermal properties of 108 half-Heuslers.

In what follows, we perform *ab initio* investigations on TE properties of two I–II–V half-Heusler compounds with eight valence electrons, KBiBa and KBiSr. The choice of these two materials is mainly due to the low values of the lattice thermal conductivity (κ_L) at 300 K found by Toher *et al* [10] (1.59 and 1.45 W m^{-1} K^{-1}). Knowing that κ_L decreases with increasing temperature, we expect low κ_L values at high temperatures, and hence a high value of the figure of merit. We start our work by identifying the most stable phase of each material. The most stable phase is examined properly by determining the electronic properties which play a significant role in thermal properties. Mechanical and dynamical stability are also examined. We perform calculations on lattice thermal conductivity, DP, elastic constant, effective mass of charge carriers and their relaxation time. The combination of these parameters allows us to determine the maximum attainable ZT and the carrier concentration at which it occurs.

2. Methods and computational details

Ab initio calculations are performed in the framework of density functional theory (DFT). The full potential linearized augmented plane-wane method with the generalized gradient approximation of Perdew–Burke–Ernzerhof (GGA-PBE) [11] is used as implemented in the Wien2k code [12]. Tran and Blaha modified Becke–Johnson potential (TB-mBJ) [13, 14] is added to spin–orbit coupling (SOC) calculations to obtain an accurate value of the bandgaps. The cutoff parameter $R_{MT} \times K_{max}$ is chosen equal to 7.0 and the energy convergence condition is achieved for 10^{-4} Ry. The muffin-tin spheres radii (R_{MT}) of each atom are 1.8, 2.1, 2.5 and 2.8 for K, Sr, Ba and Bi, respectively. A 13 × 13 × 13 *k*-mesh sampling under the Monkhorst–Pack scheme [15] is adopted for both structural and electronic properties calculations. In order to calculate TE properties of these materials, semi-classical Boltzmann equation is used as implanted in the BoltzTrap code [16]. To obtain good results, we increased the *k*-mesh sampling in the Brillouin zone to 36 × 36 × 36. The phonon dispersion calculations are performed using the plane-wave self-consistent field package implanted in the quantum ESPRESSO code [17]. A 8 × 8 × 8 mesh for the first Brillouin zone sampling and 80 Ry for cutoff of the plane wave basis set are used. The fully-relativistic ultrasoft pseudopotentials which includes SOC with the exchange-correlation part treated in the generalized gradient approximation by Perdew–Burke–Ernzerhof (GGA-PBE) [11] are used.

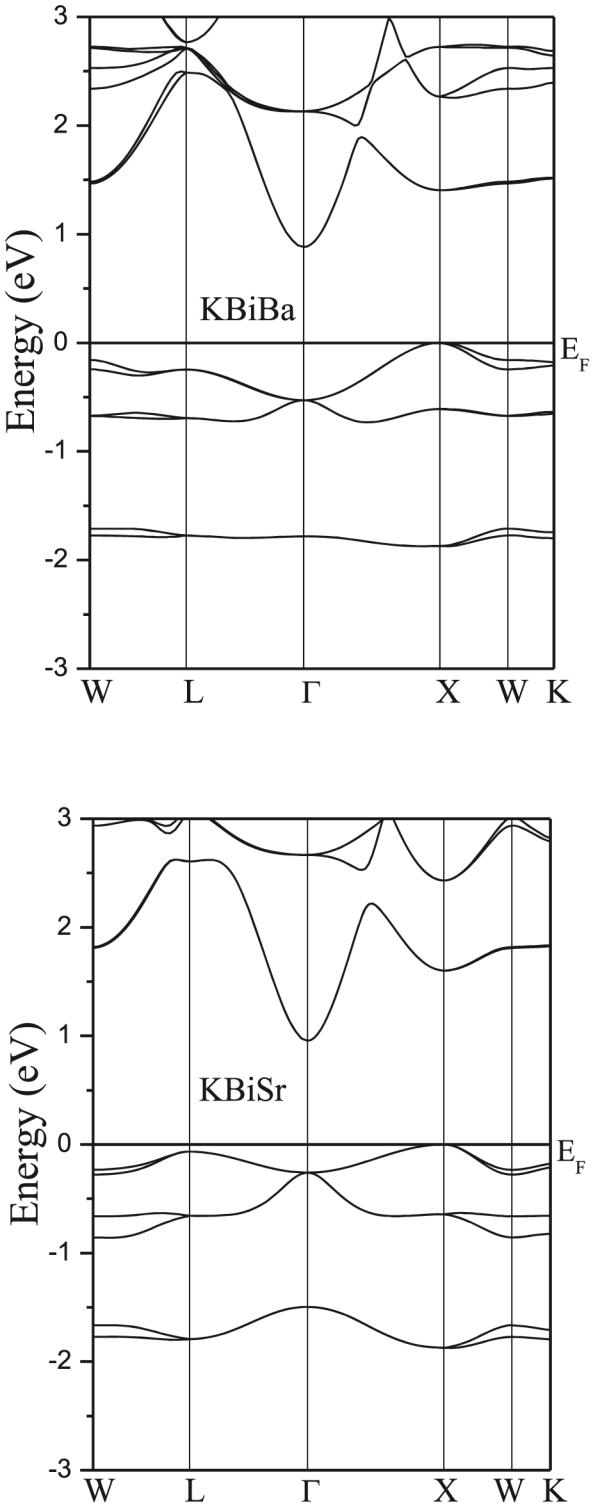

Figure 3. SOC + TB-mBJ electronic band structures of KBiBa and KBiSr.

Table 2. Elastic constants, density, longitudinal and transversal phonon velocities, bulk and shear modulus and Debye temperature of KBiBa and KBiSr.

Compound	C_{11} (GPa)	C_{12} (GPa)	C_{44} (GPa)	ρ(g cm^{-3})	v_l (m s^{-1})	v_t (m s^{-1})	B (GPa)	G (GPa)	Θ_D (K)
KBiBa	30.78	10.41	7.35	4.31	2565.11	1394.13	17.20	8.38	126.15
KBiSr	32.50	10.61	8.38	4.06	2732.52	1515.02	17.91	9.33	140.52

3. Results and discussion

3.1. Structural optimization and electronic band structures

Half-Heusler compounds have general chemical formula XYZ and crystallize in a cubic structure (space group $F\bar{4}3m$). X, Y and Z atoms occupy respectively the Wyckoff positions 4a (0, 0, 0), 4c $\left(\frac{1}{4}, \frac{1}{4}, \frac{1}{4}\right)$, and 4$b$ $\left(\frac{1}{2}, \frac{1}{2}, \frac{1}{2}\right)$. The 4$c$ site is unique in the structure where Y atom is surrounded by eight nearest-neighbors atoms. The exchange of the X and Z atoms between 4a and 4b positions does not change the structure. The total energy as function of the volume, $E(V)$, using SOC calculations was carried out for three phases called α, β, and γ depending on whether Bi, Ba (or Sr), and K are on the unique site respectively (see figure 1).

The $E(V)$ curves of the three phases for both KBiBa and KBiSr compounds are presented in figure 2. We found that the α-phase is the ground state structure of both KBiBa and KBiSr where the unique site is occupied by Bi atom. The corresponding structural parameters are obtained by fitting the total energy curves using the Murnaghan equation of states [18]. The calculated values are summarized in table 1. A favorable agreement is noticed with the recent theoretical calculation of Han *et al* [19].

In figure 3, we plot the band structures of KBiBa and KBiSr obtained by SOC + TB-mBJ calculations. The band structures display a semiconductor character with an indirect bandgap. They exhibit flat and dispersive bands at a maximum valence band with an indirect (X–Γ) bandgaps of 0.88 and 0.95 for KBiBa and KBiSr, respectively. Regarding the gap widths, the largest bandgap is obtained for SOC + TB-mBJ calculation (see table 1). The bandgap values (0.88 and 0.95) of KBiBa and KBiSr compounds calculated with SOC + mBJ approximation are different from those found by Guo *et al* (0.70 and 0.49 eV) [2]. The stable phase used (Ba and Sr occupy the single site) is different from the stable alpha phase found in our calculations (where Bi occupy the single site). Besides, the bandgap calculations are performed by the projector augmented wave scheme within GGA-PBE and without considering SOC + mBJ approximation.

On the other hand, Han *et al* [19] found a band gap value of 0.75 eV for the KBiBa compound using the hybrid functional of Heyd–Scuseria–Ernzerhof (HSE) taking into account the SOC but without considering mBJ approximation. This value is lower than that found in our calculations (0.88 eV), due to the mBJ correction which was not considered in reference [19].

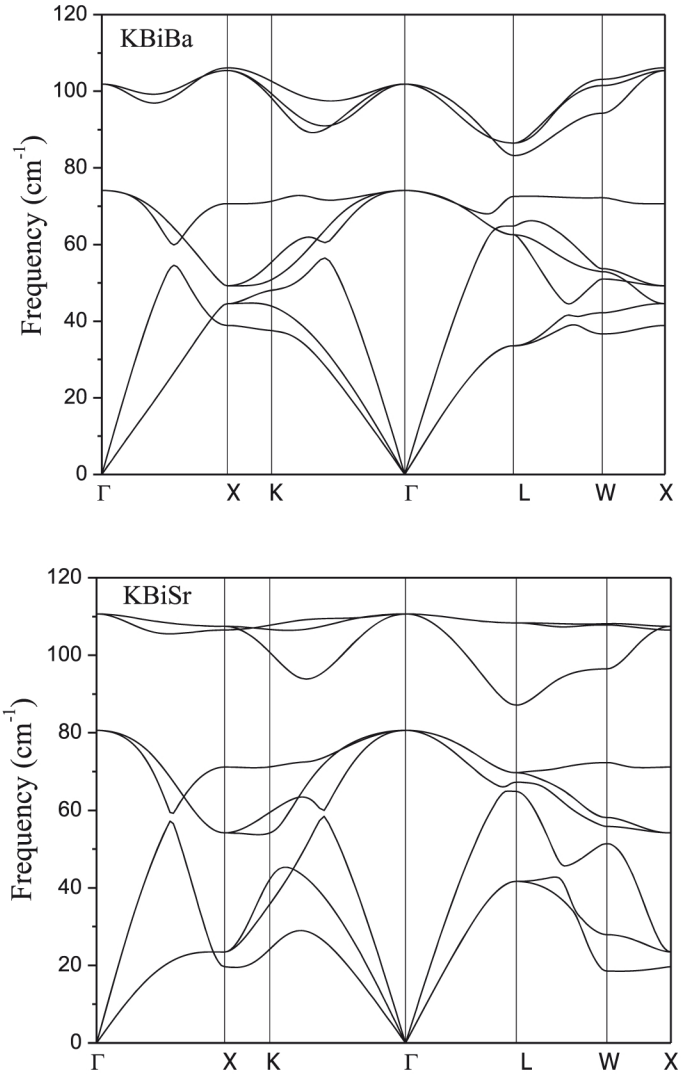

Figure 4. Phonon frequencies dispersion curves of KBiBa and KBiSr in α phase.

3.2. Mechanical and dynamical stabilities

Mechanical stability of a cubic crystal can be determined by the Born stability criteria [20], given by:

$$C_{11} - C_{12} > 0, C_{11} > 0, C_{11} + 2C_{12} > 0 \quad \text{and} \quad C_{44} > 0. \tag{1}$$

Where C_{11}, C_{12}, and C_{44} are the elastic constants. The calculated elastic constants of KBiBa and KBiSr compounds satisfy the stability conditions (see table 2), which implies that these materials are mechanically stable. The elastic constants are

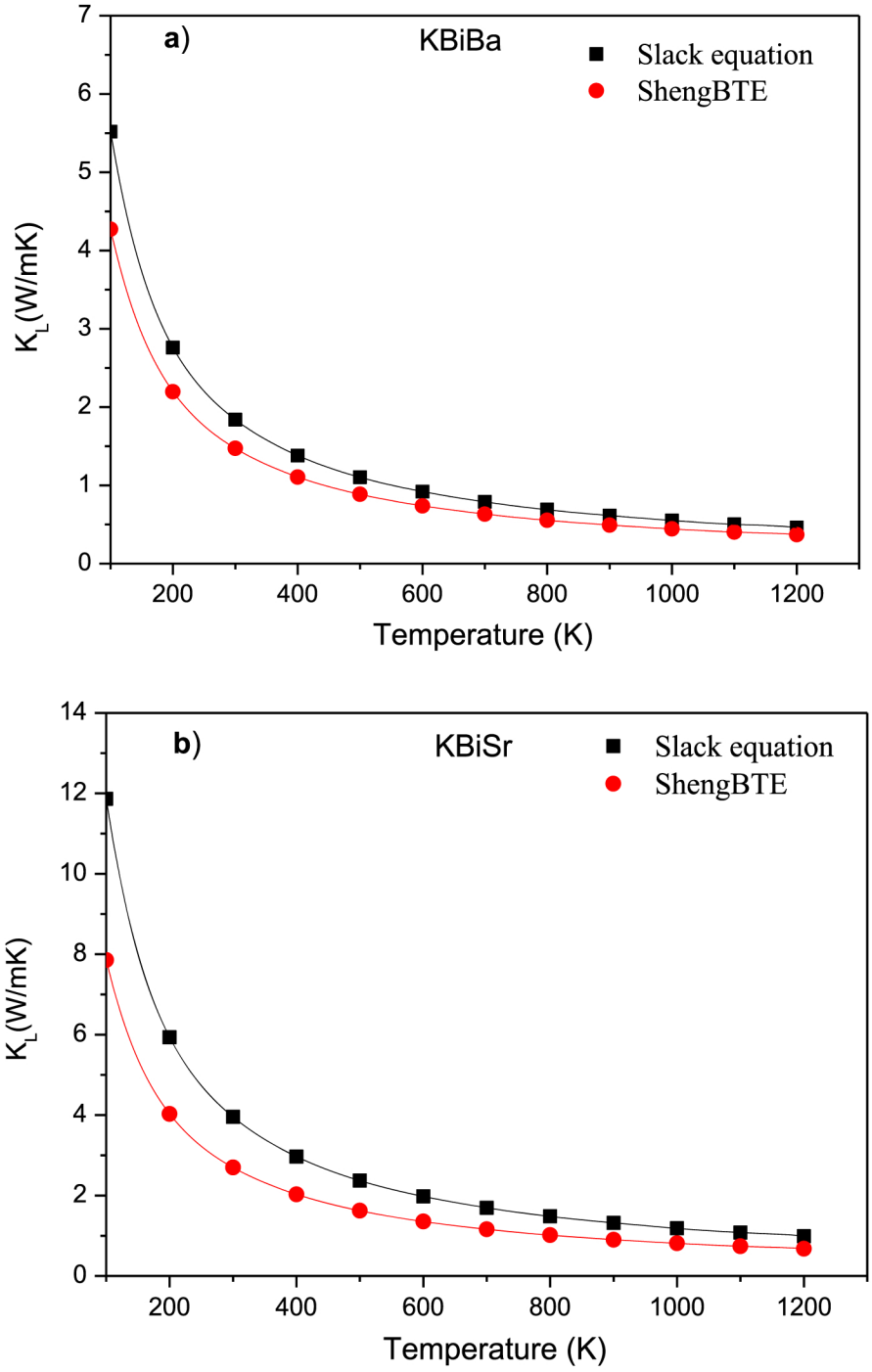

Figure 5. Temperature dependence of the lattice thermal conductivity for (a) KBiBa and (b) KBiSr using both Slack equation and ShengBTE code.

also used to determine the mechanical properties of the crystal, such as bulk modulus $B = (C_{11} + 2C_{12})/3$, shear modulus (G) and Debye temperature (θ_D). Additional information could be extracted on the brittleness or the ductility of the material by calculating the Pugh's ratio B/G [21]. According to the Voigt–Reuss–Hill approximations, G is expressed as [22–24]:

$$G = \frac{\frac{C_{11}-C_{12}+3C_{44}}{5} + \frac{5(C_{11}-C_{12})C_{44}}{3(C_{11}-C_{12})+4C_{44}}}{2}. \quad (2)$$

The Debye temperature θ_D can be estimated using Anderson's formula [25].

$$\theta_D = \frac{h}{k_B}\left(\frac{3n}{4\pi}\frac{\rho N_A}{M}\right)^{1/3}\left(\frac{1}{3}\left[\frac{1}{v_l^3} + \frac{2}{v_t^3}\right]\right)^{-1/3}. \quad (3)$$

Where h is the Planck constant, n is the number of atoms per formula unit, ρ is the density, N_A Avogadro's number, k_B is the Boltzmann constant and M the atomic mass of the unit crystal cell. v_l and v_t are the longitudinal and the transversal sound velocity, respectively, given by [25]:

$$v_t = \sqrt{G/\rho} \quad \text{and} \quad v_l = \sqrt{\frac{1}{\rho}\left(B + \frac{4}{3}G\right)}. \quad (4)$$

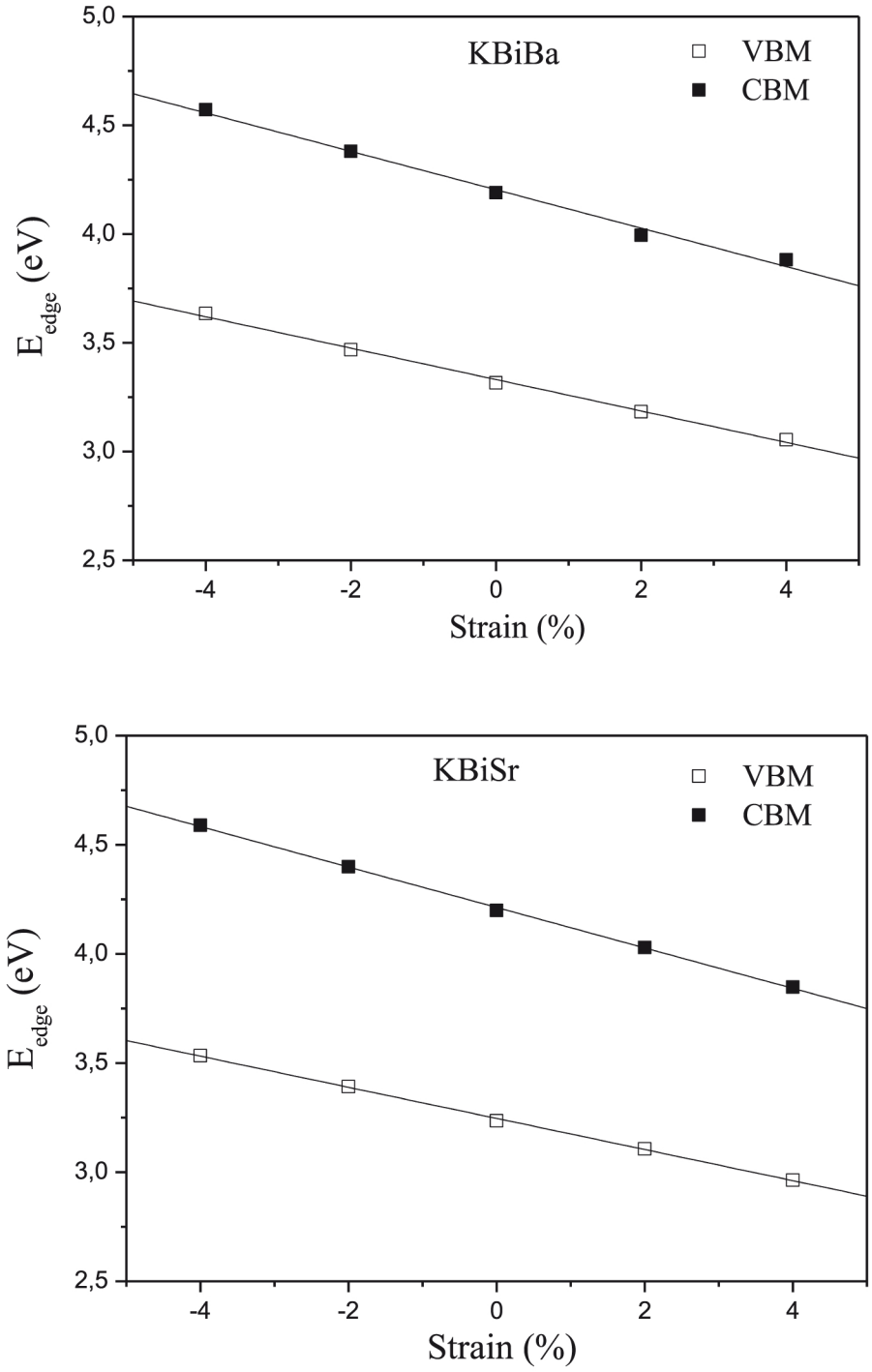

Figure 6. Band edge energy as a function of uniaxial strain for KBiBa and KBiSr.

Table 2 summarizes the calculated elastic constants and their derived mechanical parameters. The calculated bulk modulus B values from elastic constant are very close to those obtained from the Murnaghan fit (see table 1), which confirms the accuracy of our elastic constants values. The resistance to plastic deformation can be measured by the shear modulus G, the low values of G/B ratio indicate that these materials have low resistance against shear deformation.

The Pug ratios of KBiBa and KBiSr (2.05 and 1.91) exceed 1.75, which indicates that these compounds are ductile in nature favoring their use in TE applications.

Dynamical stability is established by the phonons frequencies dispersion curves along the high symmetries points. The dispersion curves of KBiBa and KBiSr in the α phase is shown in figure 4. The three atoms per unit cell give rise to nine vibrational modes, in which three of them are acoustic (low-frequency region) and six are optical (high-frequency region) modes. All phonon branches are free from negative values, confirming the dynamical stability of both compounds. Phonons are characterized by their group velocities given by the following relation $v_g = \frac{d\omega}{dq}$ which corresponds to the slope of their branches. The optical phonons branches are almost flat (their group velocities are low), while the longitudinal acoustic phonon branch, for which the variation is linear, has the highest group velocity, contributing mainly in the thermal conduction.

3.3. Thermal conductivity and thermoelectric properties

Seebeck coefficient (S), electrical conductivity (σ), electronic thermal conductivity (κ_e) and figure of merit (ZT) of KBiBa and KBiSr compounds are investigated. The lattice thermal conductivity (κ_L) is calculated by using the Slack equation and the ShengBTE code [26] based on the harmonic and anharmonic interatomic force constants combined with a full solution of phonon Boltzmann transport equation. Assuming that heat is conducted by acoustic phonons and following the procedure used in the reference [27], Slack equation gives [28]:

$$\kappa_L = A\frac{\overline{M}\theta_D^3 V^{1/3}}{\gamma^2 T n^{2/3}}. \quad (5)$$

Where $\overline{M}$ is the average atomic mass, V is the volume per atom and n is the atoms number in the primitive cell. γ is the Grüneisen parameter calculated by the expression proposed by Julian [29] and given by:

$$\gamma = \frac{9 - 12\left(v_t/v_l\right)^2}{2 + 4\left(v_t/v_l\right)^2}. \quad (6)$$

The constant A in Slack expression is calculated in terms of the Grüneisen parameter as:

$$A = \frac{2.43 \times 10^{-8}}{1 - \frac{0.514}{\gamma} + \frac{0.228}{\gamma^2}}. \quad (7)$$

According to Slack equation, a weak value of Debye temperature θ_D, a large Grüneisen parameter γ (indicating strong anharmonicity) and a high n give lead to a low value of the lattice thermal conductivity κ_L.

The calculated lattice thermal conductivity as a function of temperature for KBiBa and KBiSr using both Slack equation and ShengBTE code, represented by the figure 5, provide very close values. However, some discrepancies appear in the low temperatures range (especially at 100 K), that do not affect the material thermal properties since half-Heusler materials are known to be a good heat converter at high temperatures. The lattice thermal conductivity values are substantially equal in both approximations at higher temperatures and consequently the figures of merit values remain the same. From figure 5, κ_L decreases with the increasing of temperature and reaches 0.46 and 0.98 W m^{-1} K^{-1} values at 1200 K for KBiBa and KBiSr, respectively. At 300 K, the calculated values are found equal to 1.84 and 3.95 W m^{-1} K^{-1} whereas Carrete *et al* [9] found respectively 2.19 and 1.96 W m^{-1} K^{-1} using a full *ab initio* anharmonic characterization and Toher *et al* [10] estimated them, using AGL, to 1.59 and 1.45 W m^{-1} K^{-1}, respectively. A good agreement is observed for the value of KBiBa compared to the value of 1.82 found by Han *et al* [19]. Our calculated values are comparable to those of the best TE materials such as Bi_2Te_3 and Sb_2Te_3, which exhibit low lattice thermal conductivity at 300 K ($\simeq$2 W m^{-1} K^{-1}) [30].

To achieve the calculation of the total thermal conductivity ($\kappa_e + \kappa_L$), it is necessary to compute the electronic contribution (κ_e) part. With BoltzTraP code σ and κ_e are expressed in

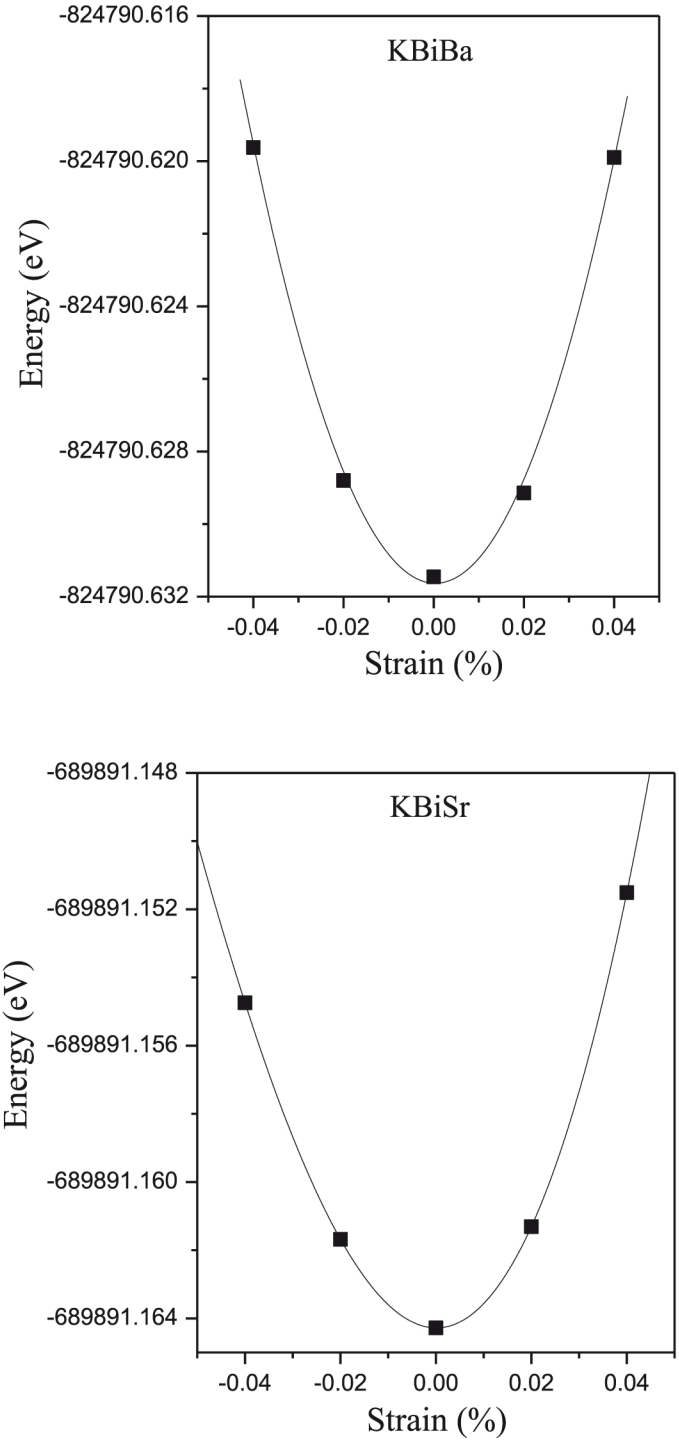

Figure 7. Total energy as a function of uniaxial strain for KBiBa and KBiSr.

Table 3. DOS effective masses, DP and elastic constant of KBiBa and KBiSr.

	Electrons			Holes		
Compound	m_d^* (m_o)	E_d (eV)	C_{ii} (GPa)	m_d^*(m_o)	E_d (eV)	C_{ii} (GPa)
KBiBa	0.27	8.83	36.29	1.35	7.22	36.29
KBiSr	0.22	9.18	36.65	1.72	7.11	36.65

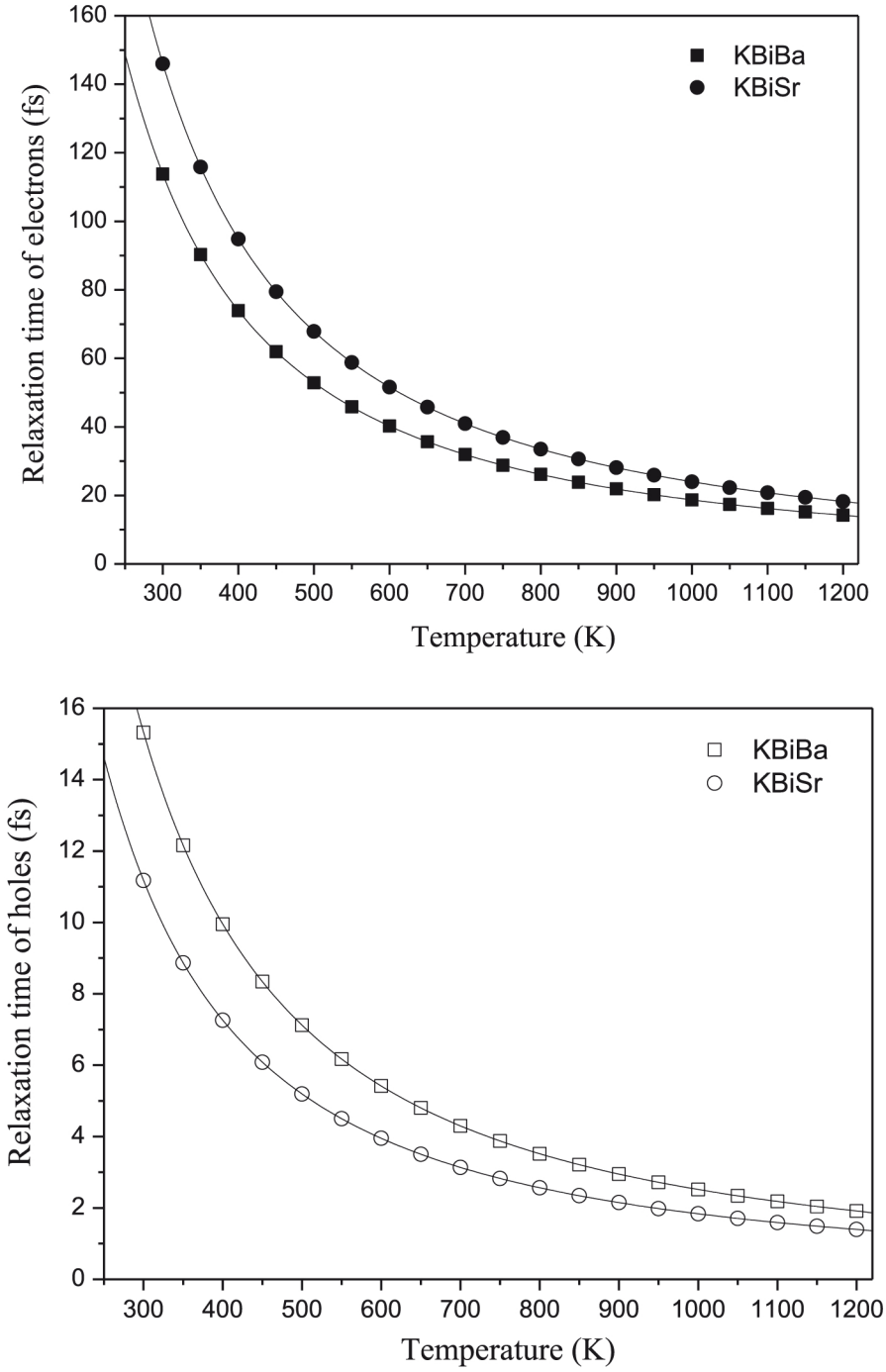

Figure 8. Holes and electrons relaxation time of KBiBa and KBiSr versus temperature.

the form of the ratios σ/τ and κ_e/τ, where τ is the electronic relaxation time estimated in this study by using the DP theory given by Bardeen and Shockly [31]. At the same temperature, we assume that the relaxation time is constant when carrier concentration changes, in this case τ is given by:

$$\tau = \frac{(8\pi)^{1/2}\hbar^4 C_{ii}}{3\left(m_d^* k_B T\right)^{3/2} E_d^2}. \tag{8}$$

Where $\hbar$ is the reduced Planck's constant, m_d^* is the de density of states (DOS) effective masse, C_{ii} is the elastic constant and E_d the DP. The latter, calculated for holes and electrons from the band edge energy of valence band maximum (VBM) and conduction band minimum (CBM) as function of the uniaxial strain $\frac{\Delta a}{a_0}$ is given by:

$$E_d = \frac{E_{edge}}{\partial\left(\frac{\Delta a}{a_0}\right)}. \tag{9}$$

Where $\Delta a = a - a_0$ is the shift from the equilibrium lattice constant a_0. The energy of the VBM and CBM vary linearly with the applied strain, as shown in figure 6. The slope of the curves represents E_d.

The elastic constants C_{ii} are computed by the quadratic polynomial fit of the total energy variation under strains as:

$$C_{ii} = \frac{1}{V_0}\frac{\partial^2 E}{\partial\left(\frac{\Delta a}{a_0}\right)^2}. \tag{10}$$

Where, V_0 is the equilibrium volume. The fitted curves versus strains of both compounds are shown in figure 7.

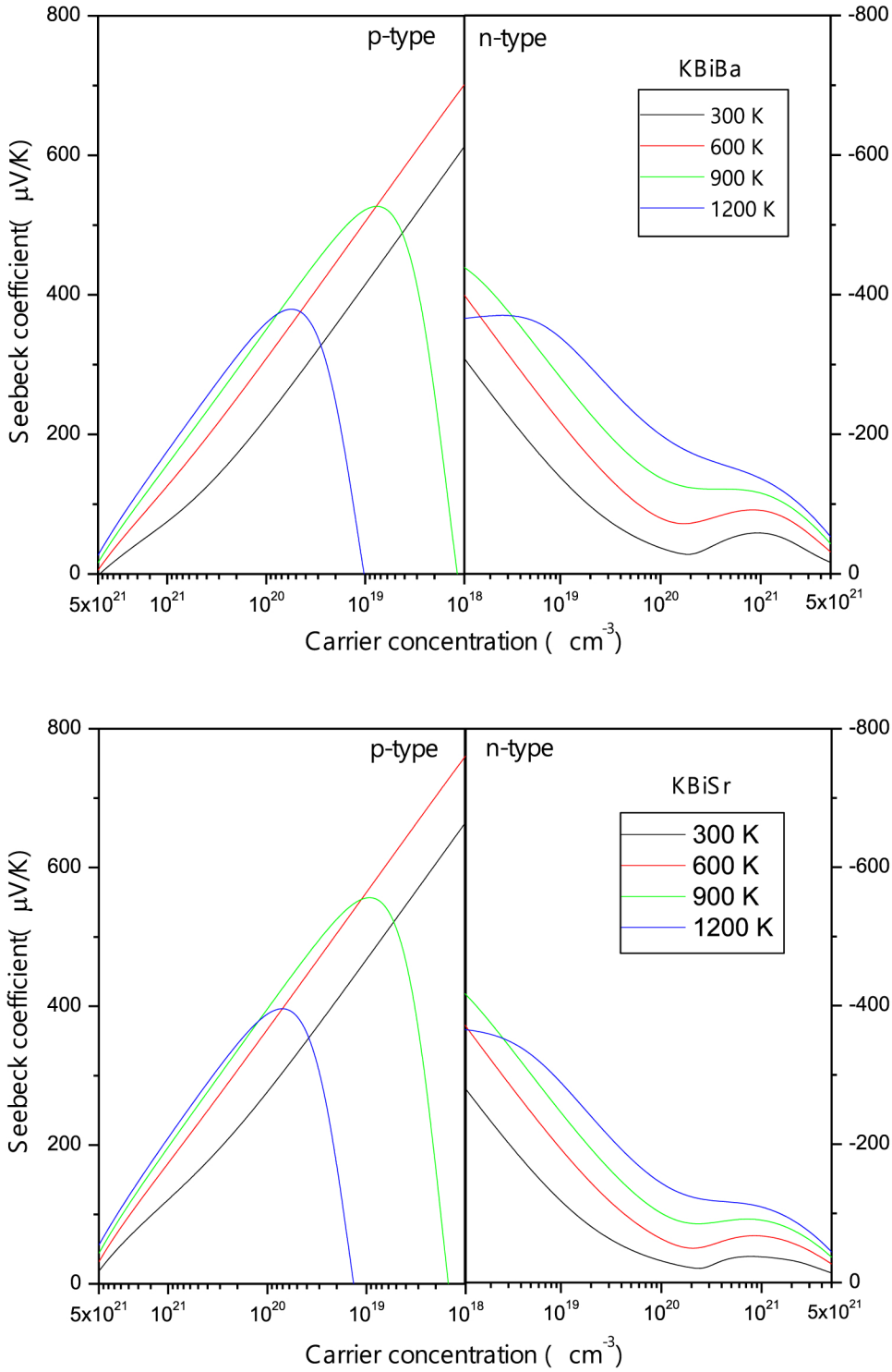

Figure 9. Seebeck coefficient of KBiBa and KBiSr as a function of carrier concentration at different temperatures.

The effective mass of charge carriers in both valence and conduction bands under the parabolic approximation is defined by the curvature of the band in k-space as:

$$m^* = \frac{\hbar^2}{\left(\frac{\partial^2 E}{\partial k^2}\right)}. \tag{11}$$

This implies that the effective mass for a flat energy curve will be greater than the narrower energy curve at a given k-point. The DOS effective mass m_{d}^*, on which the Seebeck coefficient depends, is defined as $N_v^{2/3}\left(m_x^* \cdot m_y^* \cdot m_z^*\right)^{1/3}$, where N_v is the number of bands involved in transport (band degeneracy). For an isotropic material with a same band masses $\left(m_x^* = m_y^* = m_z^* = m^*\right)$ along the x, y, z directions, $m_{\mathrm{d}}^* = N_v^{2/3} m^*$. Thus, a large N_v and a small m^*, could, simultaneously, gives rise to a high Seebeck coefficient and a high mobility [32]. The calculated values of E_{d}, C_{ii} and m_{d}^* for KBiBa and KBiSr compounds are listed in table 3.

According to the equation (8) and by using the results of m_{d}^*, E_{d} and C_{ii}, we plot in figure 8 the relaxation time

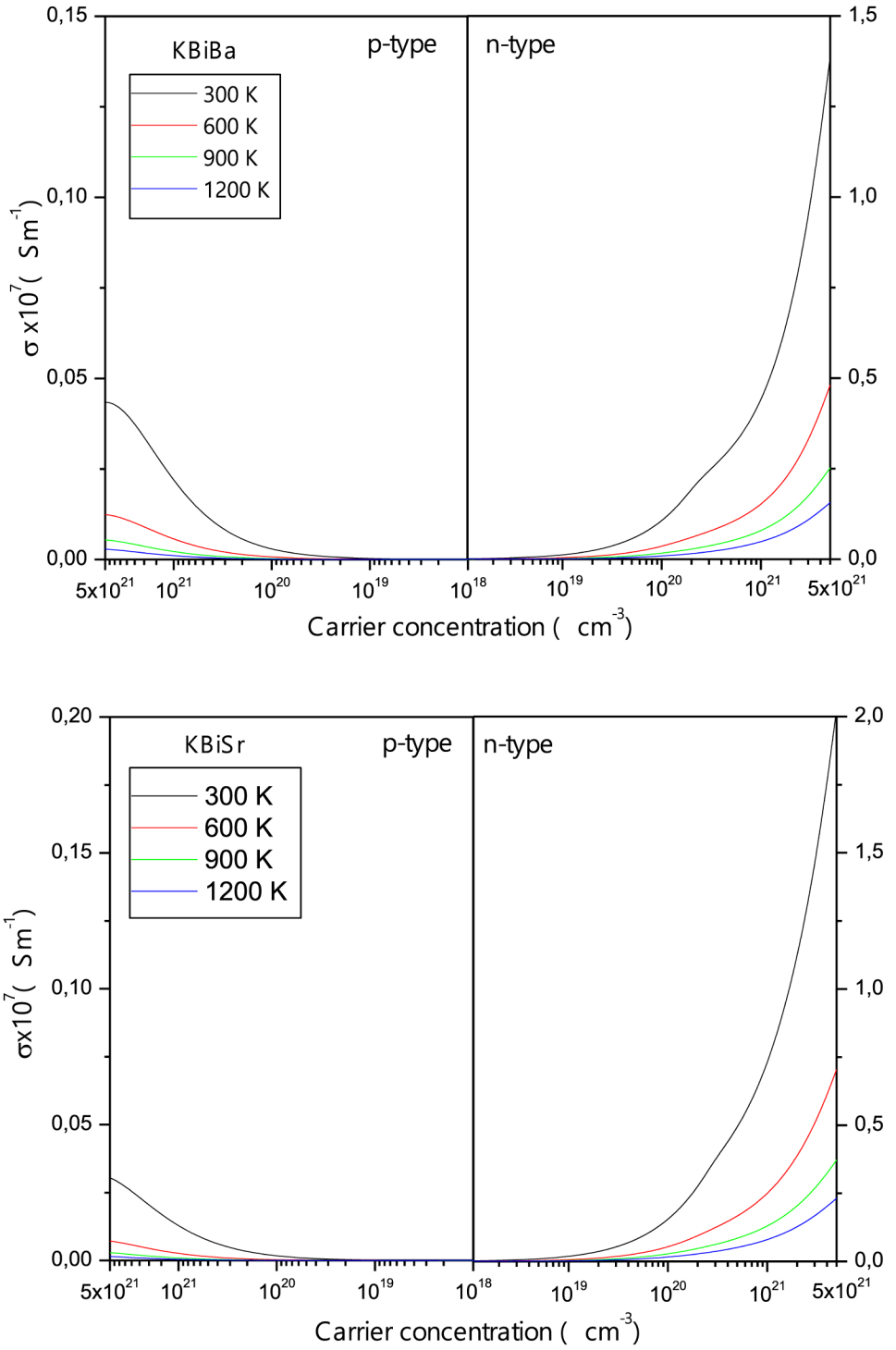

Figure 10. Electrical conductivity of KBiBa and KBiSr as a function of carrier concentration at different temperatures.

τ of both holes and electrons as a function of the temperature. The changes of relaxation times evolve in a similar way in both compounds. They undergo a strength decrease then vary slowly over a wide high temperature range. The electrons relaxation times are ten times longer than those of holes for both compounds. We, therefore, expect a high electrical conductivity and thus a high power factor in both *n*-doped compounds.

Figure 9 shows the calculated Seebeck coefficient as a function of carrier concentration at different temperatures (300, 600, 900, and 1200 K). For simple metals or degenerate semiconductors with parabolic bands and energy independent scattering, the Seebeck coefficient is given by [33]:

$$S = \frac{8\pi^2 {k_B}^2 T}{3eh^2} {m_d}^* \left(\frac{\pi}{3n}\right)^{2/3}. \quad (12)$$

For both doping types, the absolute value of S increases when the carrier concentration decreases. For the *p*-type doping and high temperature, it reaches a maximum and then decreases due to the bipolar effect. Maximum absolute values

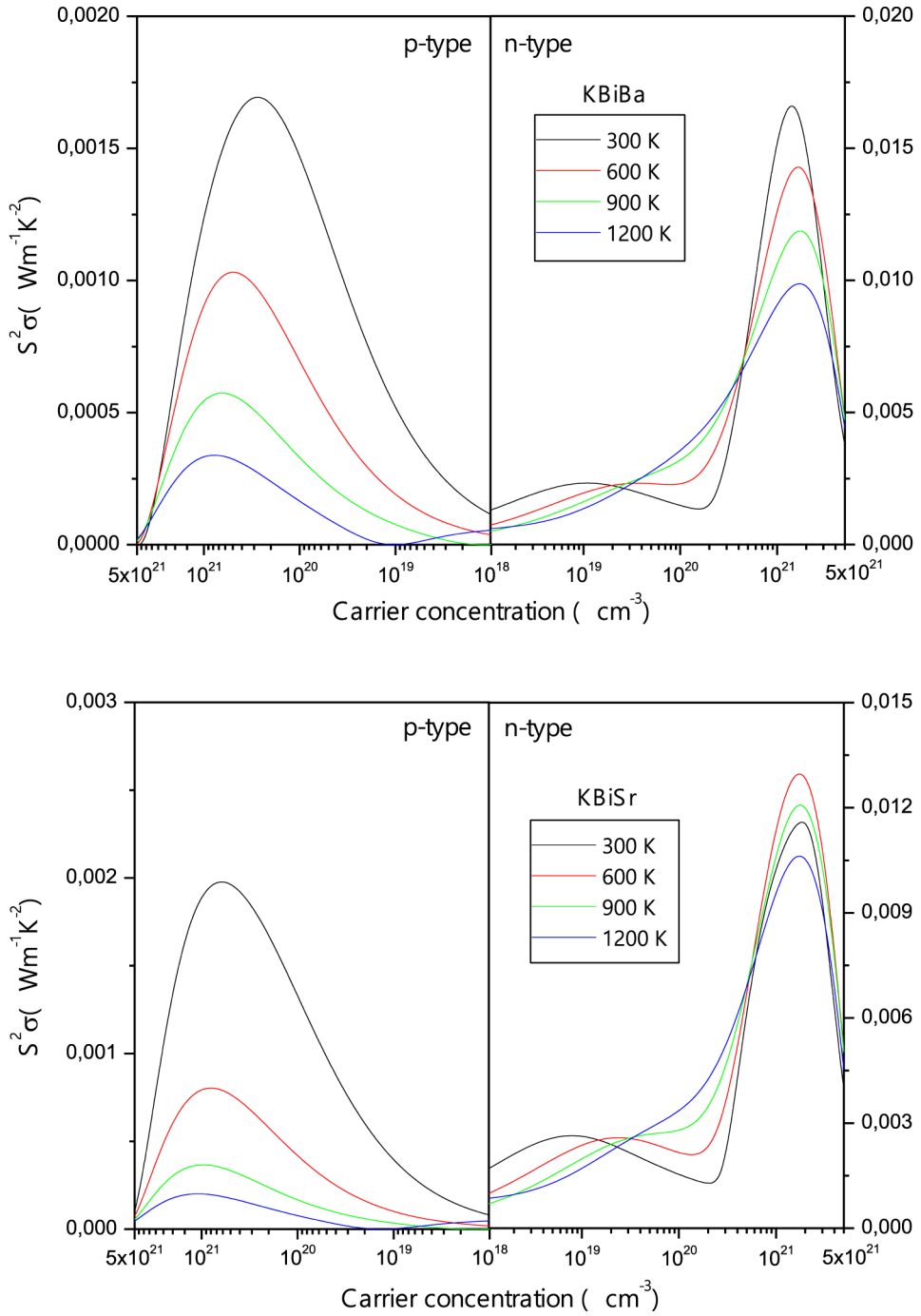

Figure 11. Power factor of KBiBa and KBiSr as a function of carrier concentration at different temperatures.

are reached in the regions of weak carrier concentration for both KBiBa and KBiSr compounds. S values of p-type doping are higher than that of n-type ones. This is related to the fact that the holes effective mass is higher than that of electrons.

Contrary to S, the electronic conductivity as shown in figure 10 increases with increasing carrier concentration. For both compounds, σ values of the n-doping are significantly larger than that of the p-doping at the same carrier concentration and temperature. This is interpreted by the fact that the conductivity is inversely proportional to the effective mass and evolves directly with the relaxation time of charge carriers. A combination of a larger relaxation time, as well as, a smaller effective mass of the electrons with respect to the holes, makes the electrons conductivity higher. In the high n-doping region, the maximum electrical conductivity reaches 1.3×10^7 S m^{-1} for KBiBa, while for KBiSr it reaches 2×10^7 S m^{-1}, both at 300 K.

Figure 11 displays the change of the power factor ($S^2\sigma$) as a function of doping concentration at various temperatures. Based on the electronic structures, these compounds exhibit dispersive valence bands and high band degeneracy, leading to a maximum n-type power factor of 16×10^{-3} W m^{-1} K^{-2} (11.6×10^{-3} W m^{-1} K^{-2}) for KBiBa (KBiSr) at 300 K. We note that the $S^2\sigma$ peaks are located in the large carrier concentration range and are absent for low concentration (10^{18}–10^{20} cm^{-3}) due to the small σ values in this region.

In order to achieve to a correct estimation of the figure of merit, the total thermal conductivity is required. κ_L was carried

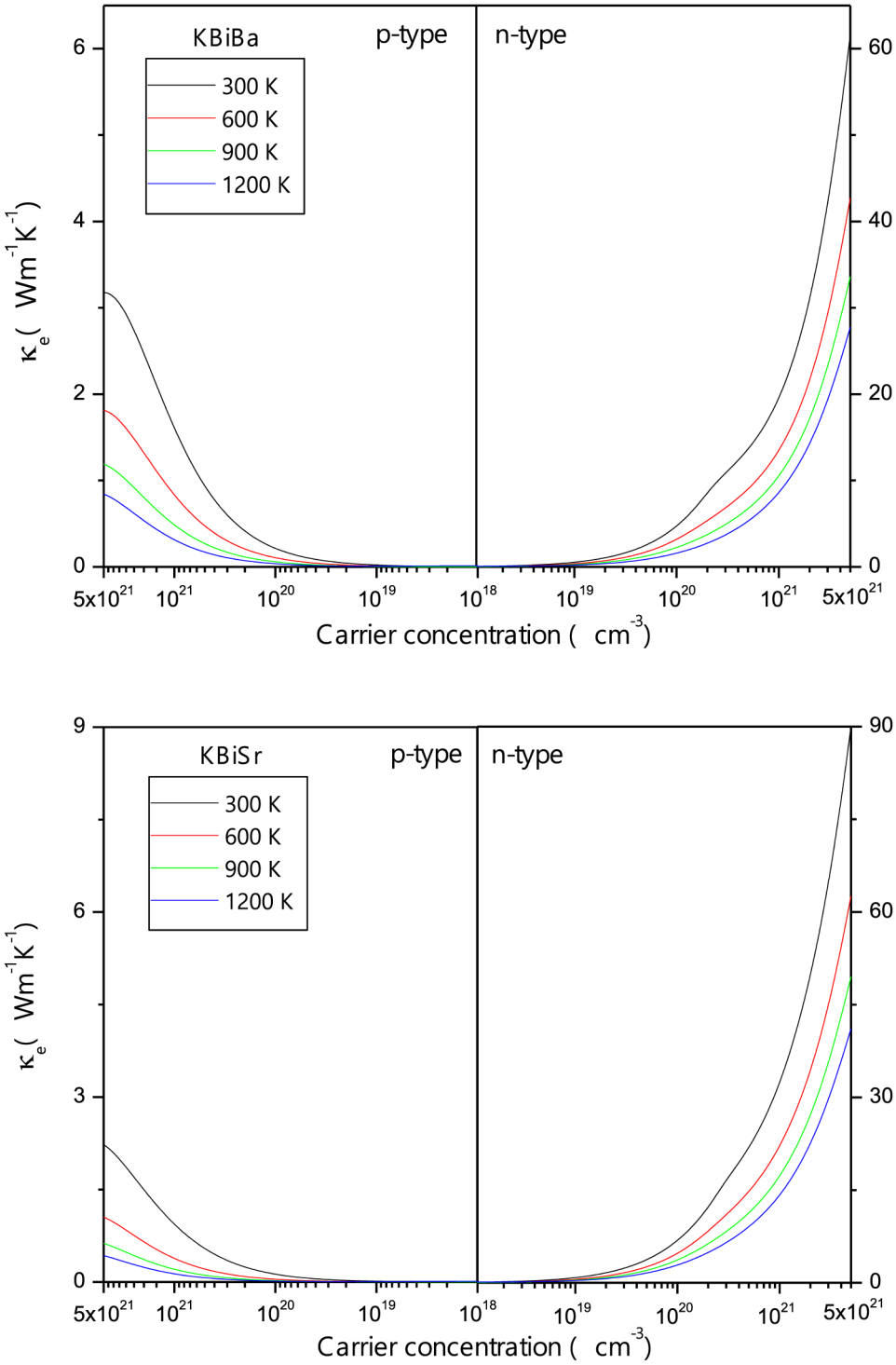

Figure 12. Electronic thermal conductivity of KBiBa and KBiSr as a function carrier concentration at different temperatures.

out previously and the electronic contribution of the thermal conductivity is estimated through the Wiedemann–Franz law $\kappa_e = L\sigma\sigma$, where L is the Lorentz number. For metals or a degenerate semiconductors, L is given by $(\pi k_B/e)^2/3$ and for nondegenerate semiconductors it is given by $2(k_B/e)^2$ [34]. κ_e is presented in figure 12 as a function of carrier concentration at various temperatures. In both doping types, the shape of the electronic thermal conductivity curves varies in the same way as those of the electrical conductivity. Also, both types of thermal conductivities decrease with increasing temperature. It is noticed that the largest κ_e values are obtained in the high doping region. For KBiBa, the κ_e values of the n-type doping carriers are 20 times (40 times for KBiSr) larger than that for the p-type ones.

By using the power factor and the total thermal conductivity results, we calculate the dimensionless figure of merit ZT as a function of the carrier concentration for various temperatures. Figure 13 shows that ZTs for n-type doping are greater than that for p-type ones. At 300 K, ZT is low and is equal to 0.31 (0.18) for KBiBa (KBiSr) reaching 2.68 (1.56) at 1200 K for the optimized n-doping value of 2.2×10^{19} cm^{-3} (1.7×10^{19} cm^{-3}). At 1200 K, a maximum ZT value of 0.61 (0.21)

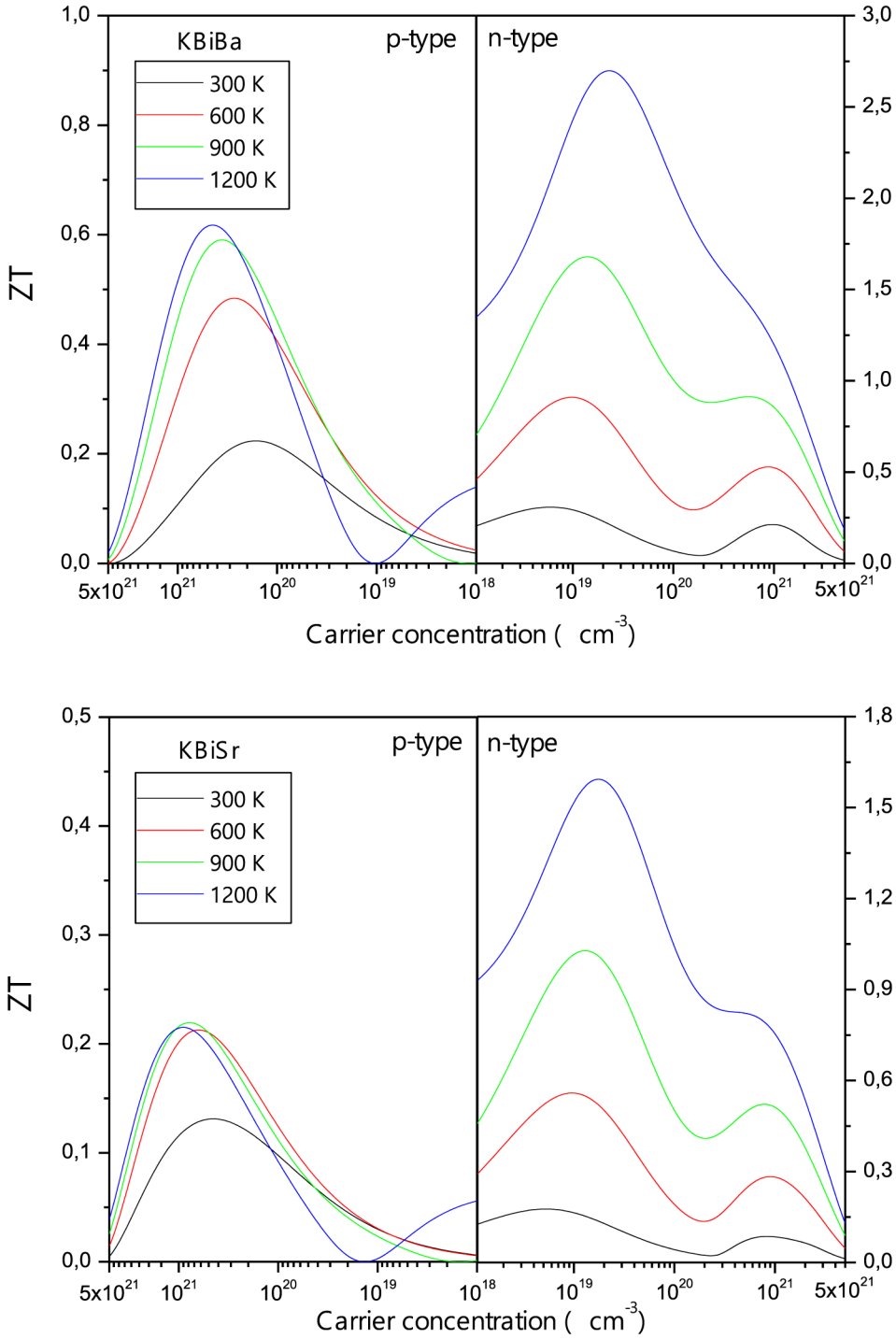

Figure 13. ZT of KBiBa and KBiSr as a function of carrier concentration at different temperatures.

is found for p-doping concentration of 4.48×10^{20} cm^{-3} and 9.15×10^{20} cm^{-3} for KBiBa and KBiSr, respectively. Han *et al* [19] have predicted, using first principle calculations, a ZT value of 1.9 for the n-doped KBiBa compound at 900 K. This value is higher than 1.7 found in our study. This is due to the fact that Han *et al* drop mBJ approximation which enhances the gap value and thus affects the ZT value.

4. Conclusion

The energetically stable phase of the half-Heusler compounds KBiBa and KBiSr is investigated using the DFT. Electronic properties, using GGA + SOC calculations combined with the TB-mBJ approximation, reveal that these compounds are p-type semiconductors with indirect gaps. The calculated elastic constants and phonons frequencies dispersion curves show that the studied compounds are mechanically and dynamically stable. The TE properties are calculated using the semi-classical Boltzmann theory. The lattice thermal conductivity κ_L at different temperatures is investigated using Slack's equation. At high temperature, κ_L is extremely low (smaller than 1 W m^{-1} K^{-1}) leading to high values of ZT, 2.68 and 1.56 at 1200 K, for n-doped KBiBa and KBiSr, respectively. On the

basis of the results KBiBa and KBiSr half-Heusler compounds could be considered as good TE materials.

Acknowledgments

This work was financially supported by the Algerian national research projects, PRFU/DGRSDT/MESRS-Algeria (project n° B00L02UN270120180001).

Data availability statement

All data that support the findings of this study are included within the article (and any supplementary files).

References

[1] Snyder G J and Toberer E S 2008 *Nat. Mater.* **7** 105
[2] Guo S, Jia T and Zhang Y 2019 *J. Phys. Chem.* C **123** 18824
[3] Fu C, Bai S, Liu Y, Tang Y, Chen L, Zhao X and Zhu T 2015 *Nat. Commun.* **6** 8144
[4] Fang T, Zheng S, Zhou T, Yan L and Zhang P 2017 *Phys. Chem. Chem. Phys.* **19** 4411
[5] Ahmed R, Masuri N S, Ul Haq B, Shaari A, AlFaifi S, Butt F K, Muhamad M N, Ahmed M and Tahir S A 2017 *Mater. Des.* **136** 196
[6] Sun H-L, Yang C-L, Wang M-S and Ma X-G 2020 *ACS Appl. Mater. Interfaces* **12** 5838
[7] Yang C L, Wang M S, Ma X G and Zhang Q 2021 *Mater. Today Commun.* **26** 101971
[8] Yang J, Li H, Wu T, Zhang W, Chen L and Yang J 2008 *Adv. Funct. Mater.* **18** 2880
[9] Carrete J, Li W and Mingo N 2014 *Phys. Rev.* X **4** 011019
[10] Toher C, Plata J J, Levy O, De Jong M, Asta M, Nardelli M B and Curtarolo S 2014 *Phys. Rev.* B **90** 174107
[11] Perdew J P, Burke K and Ernzerhof M 1997 *Phys. Rev. Lett.* **78** 1396
[12] Blaha P, Schwarz K, Sorantin P and Trickey S B 1990 *Comput. Phys. Commun.* **59** 399
[13] Tran F, Blaha P and Schwarz K 2007 *J. Phys.: Condens. Matter* **19** 196208
[14] Tran F and Blaha P 2009 *Phys. Rev. Lett.* **102** 226401
[15] Monkhorst H J and Pack J D 1976 *Phys. Rev.* B **13** 5188
[16] Madsen G K H and Singh D J 2006 *Comput. Phys. Commun.* **175** 67
[17] Giannozzi P *et al* 2009 Quantum ESPRESSO: a modular and open-source software project for quantum simulations of materials *J. Phys.: Condens. Matter* **21** 395502
[18] Murnaghan F D 1944 *Proc. Natl Acad. Sci. USA* **30** 244
[19] Han S H, Zhou Z Z, Sheng C Y, Liu J H, Wang L, Yuan H M and Liu H J 2020 *J. Phys.: Condens. Matter* **32** 425704
[20] Born M and Huang K 1954 *Dynamical Theory of Crystal Lattices* (Oxford: Oxford University Press)
[21] Pugh S F 1954 *Phil. Mag.* **45** 823
[22] Voigt W 1928 *Lehrbuch der Kristallphysik* (Leipzig: Teubner)
[23] Reuss A 1929 *Z. Angew. Math. Mech.* **9** 55
[24] Hill R 1952 *Proc. Phys. Soc.* A **65** 349
[25] Anderson O L 1963 *J. Phys. Chem. Solids* **24** 909
[26] Li W, Carrete J, A. Katcho N and Mingo N 2014 *Comput. Phys. Commun.* **185** 1747
[27] Cherifi F, Mostefa Z, Boukra A, Meghoufel Z F, Bouattou M, Kadi Allah F and Terki F 2020 *Phys. Status Solidi b* **257** 2000271
[28] Slack G A 1973 *J. Phys. Chem. Solids* **34** 321
[29] Julian C L 1965 *Phys. Rev.* **137** A128
[30] Toberer E S, Zevalkink A and Snyder G J 2011 *J. Mater. Chem.* **21** 15843
[31] Bardeen J and Shockley W 1950 *Phys. Rev.* **80** 72
[32] Pei Y, Shi X, LaLonde A, Wang H, Chen L and Snyder G J 2011 *Nature* **473** 66
[33] Felser C and Fecher G H 2013 *Spintroincs: From Materials to Devices* (Berlin: Springer)
[34] Spitzer D P 1970 *J. Phys. Chem. Solids* **31** 19